Journal of Materials Science: Materials in Electronics (2018) 29:13277–13285
https://doi.org/10.1007/s10854-018-9451-z

Preparation and characterization of $LiCo_{0.5}Ni_{0.45}Ag_{0.05}O_2$ cathode material for lithium–ion battery

Adawiya J. Haider[1] · Ahmed A. Al-Tabbakh[2] · Aseel B. Al-Zubaidi[3] · Rusul A. Rsool[1]

Received: 25 April 2018 / Accepted: 8 June 2018 / Published online: 11 June 2018

Abstract
In this work, the layered compound of $LiCo_{0.5}Ni_{0.45}Ag_{0.05}O_2$, (LCNAO) was prepared by self-propagating combustion reaction for the cathode of lithium–ion battery. The as-synthesized material was subjected to thermo-gravimetric (TGA) analysis to determine the optimum range of annealing temperatures. Accordingly were annealed at 800, 900 and 1000 °C for 8 h in air and changes in the structural and morphological properties were studied. The structural properties of LCNAO powder were studied by means of X-ray diffraction (XRD), Field emission Scanning Electron Microscopy (FE-SEM), Energy Dispersive Spectrometry (EDS), Atomic Force Microscopy (AFM) and a vibrating samples magnetometer (VSM). XRD analysis shows that all the powders are crystallized in the Phase structure R-3m and present a random orientation and surface morphology of the LCNAO powder consists of Nano-crystalline grains with uniform coverage of the substrate surface with randomly oriented. Hysteresis behavior analysis that the possessed soft magnetic properties. Thermo-gravimetric analysis show that the best annealing temperature and duration that leads to particles in the range 86–103 nm of the targeted composition are 900 °C for 8 h.

1 Introduction

Energy plays a very important role in the life. Factors such as pollution, global warming and Limited resources of conventional energy supplies make this, together with the utilization of renewable energy, a worldwide priority [1]. Hybrid electrical vehicles and electric cars are being used increasingly [2]. The main objective of global energy sustainability aims at the interchange of all fossil fuels (oil, coal, natural gas) with renewable energy sources (geothermal, hydrogen, batteries, etc.). The cathode elements for lithium batteries include oxygen and a transition element is their chemical formula. The transition ion is magnetic (with only few exceptions like Ag^{1+} of Co^{3+} in the low-spin state). In addition, the materials are often semiconductors with small electron (or hole) concentration, so that the magnetic exchange interactions are essentially super exchange interactions that are short range [1–3]. That is why it is an important tool to characterize the sample, by detecting impurity phases or local defects. It comes in complement to other more conventional tools. Many researchers have used Manganese and iron in the preparation of cathode for lithium–ion batteries and have succeeded in improving its properties [4–6]. This is usually achieved by using heavy ions of transition metals to maintain the inter-atomic during intercalation and de-intercalation processes [2, 7]. Silver has rarely been examined in cathode active compounds of lithium–ion batteries for being costly in battery industry. Nevertheless, since low doping is adequate Alter the structural stability as well as the electrochemical performance of the material it is worthwhile to investigate the effect of silver on the cathode compounds for energy storage applications [8]. For lithium–ion batteries, $LiCoO_2$ is the most commonly used cathode material due to its high capacity and good cyclability [9].

Wet-chemistry refers to a synthesis technique which involves using a liquid phase and acidification of aqueous solutions of the starting materials. Such techniques are classified in four groups according the salts and complexing agent applied. They are namely sol–gel [2, 6], co-precipitation [7, 8], combustion [9], pyrolysis [10], polyol [11]

✉ Adawiya J. Haider
amer.aljoburi@yahoo.com

[1] Department of Applied Science, University of Technology, Baghdad 10066, Iraq

[2] Department of Physics, Al-Nahrain University, Jadiriya, Baghdad 64055, Iraq

[3] Department of Materials Engineering, University of Technology, Baghdad, Iraq

etc. These techniques were used to prepare nano-structured metal oxides used in the cathodes of Li–ion batteries [3, 12].

Excellent reviews describing molecular structure, thermal and electrochemical stabilities and electrochemical performance of lithiated manganese oxide and other derivatives are available in the literature [1, 13]. Nevertheless, parallel investigations of topographical structure and its dependence on thermal treatment of the material is not thoroughly achieved and made available.

In this study, we developed and improved the preparation of LCNAO through a simple and economical method of combustion reaction in the air and include an exothermic reaction of oxidant (metal nitrate) and organic fuel to get the desired configuration. Also, the silver added in the preparation of the lithium–ion cathode has improved its properties.

2 Experimental work

$LiNO_3$, $Co(NO_3)_2{\cdot}6H_2O$, $Ni(NO_3)_2{\cdot}6H_2O$, $Ag(NO)_3$, $C_6H_6O_7$ of high purity (99/99%) were procured from Harris Chemicals Corporation in England. 14% of $LiNO_3$, 29.57% of $Co(NO_3)_2{\cdot}6H_2O$, 26.60% of $Ni(NO_3)_2{\cdot}6H_2O$, 1.72% of $Ag(NO)_3$, were used as precursors All nitrates were dissolved in deionized water and kept under magnetic stirring for 15 min at room temperature. The solution was then heated on hot-plate for 30 min [14–16]. The combustion reaction is a chemical reaction that depends on the fuel material and the purity of the starting reactants. Figure 1 illustrated steps of procurer the combustion reaction.

The first step of the combustion reaction is the evaporation of the water and increase of viscosity [5, 6, 17]. Combustion of the mixture starts after reducing the water constituent of the solution to a critical point and raising of temperature to the threshold value; the value at which an amount of energy is supplied to initiate the reaction. Figure 2 shows the reaction vessel before, during and after the combustion. The as-synthesized material was collected in powder-like form and subjected to further processing and characterization.

Figure 3 shows the reaction route in a schematic diagram. The first step of the reaction is the formation of metals, hydroxides, and nitric acid from the metals nitrates dissolved in water. The second step is formation of intermediate compounds, due to addition of citric acid and reaction of the metal carboxyl with the nitric acid during the combustion of the mixture. The proposed route indicates that the addition of $Ag(NO)_3$ may result into the formation of Ag OH or Ag_2O_3 both of which are believed to lead to inserting Ag in the layered structure of the final product, which is composed of the lithiated metal oxide as ($LiCo_{0.5}Ni_{0.45}Ag_{0.05}O_2$), CO, N_2 and water [14, 16].

Thermal analysis of the powder sample was made using thermo-gravimetric (TG) analyzer STA-PT1000 TG from Lenses Germany. The heating rate was set at 25°/min while atmospheric pressure was maintained during the measurements. The aim of the thermal analysis is to find the optimum temperature at which elimination of contaminants and phase formation along with crystallization take place.

The LCNAO powders were analyzed by the X- ray diffraction (XRD-6000) using 2ɵ, operating, 40 kV and 30 m, X-ray Cu Kα (1.540600 Å). The Topographies were investigated on Field Emission Scanning Electron Microscope (FE-SEM); MIRA3 TESCAN. The compositional properties of the material were investigated by XEPOS X-ray energy dispersive spectrometer. The particle size distribution of this statement atomic force microscope (Angstrom USA, Spm3000 AFM system). The measurements were performed in the contact mode of the microscope. The 3D images are very important technique to investigate the surface topography of the powder. The magnetic properties determined by a vibrating sample magnetometer VSM (Model VSMF 7407).

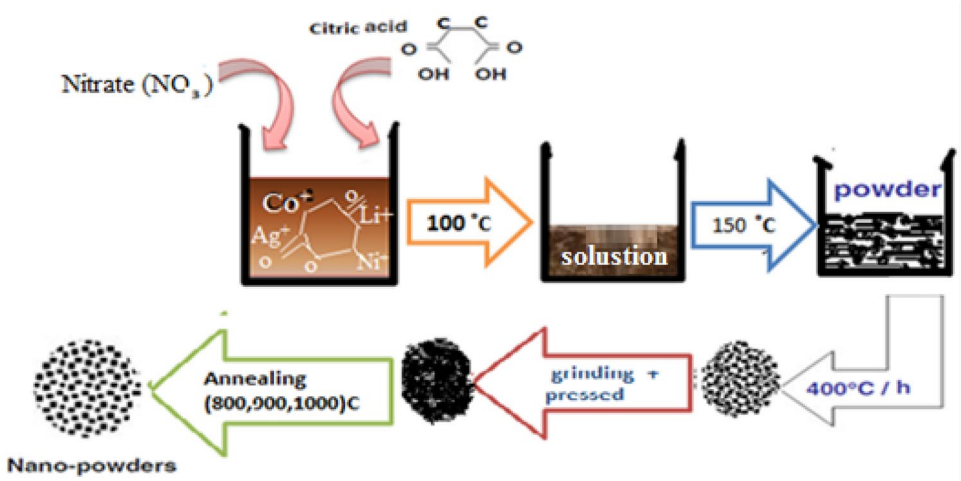

Fig. 1 Schematic of combustion reaction

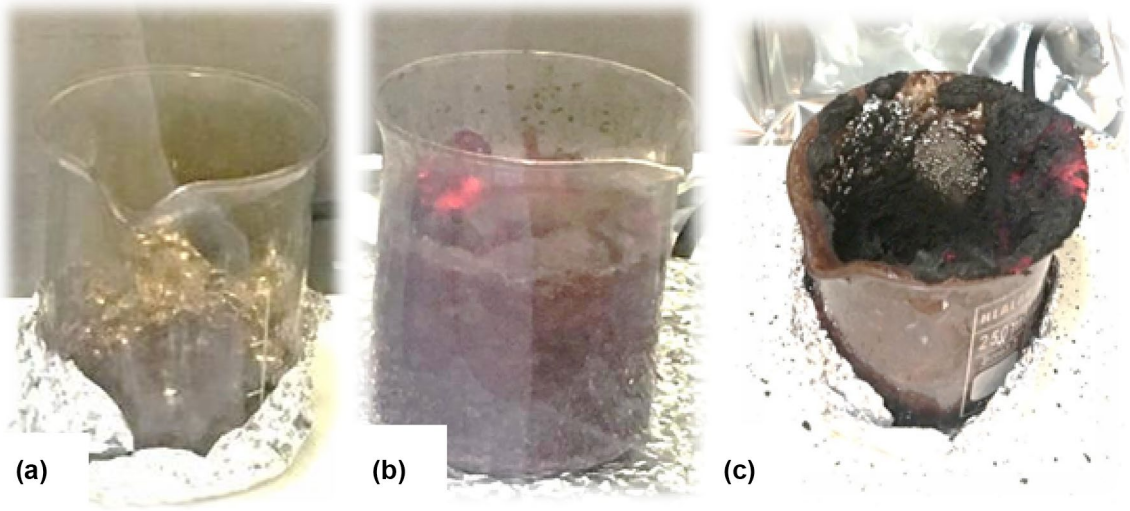

Fig. 2 Vessel of the combustion reaction **a** before combustion, **b** during and **c** after combustion was completed

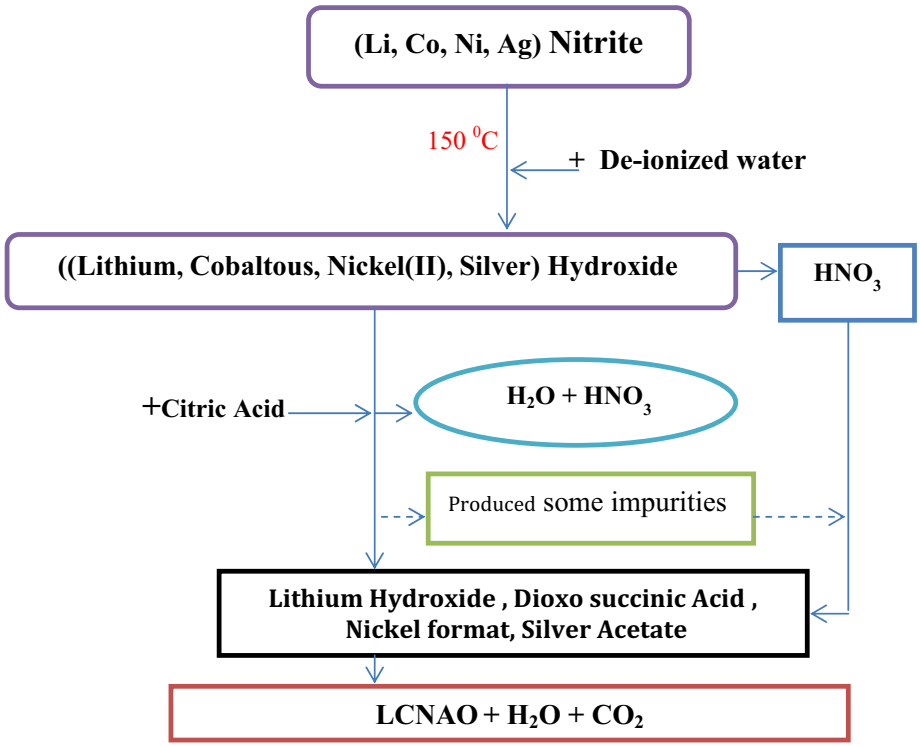

Fig. 3 The steps of the formation of the cathode material by combustion

3 Results and discussion

TG measurements are shown in Fig. 4. The mass loss curve exhibited a continuous decrease of mass with temperature. With reference to the heat flow curve, three points on the mass-loss plot were selected for further analysis. The First weight loss at 100 °C accompanied with endothermic peak was due to the evaporation of residual water from the as-synthesized material. The second mass loss took place at about 541 °C at which an exothermic peak, associated with further combustion of the unreacted materials. The Third point occurred at 700 °C where a pure phase of the material formed [2, 5–19]. It is expected that, lithium oxide are decomposed at annealing temperatures higher than 850 °C. However, a structurally better compound is believed to be formed at these high temperatures provided that the heat treatment does not last for long hours (Table 1).

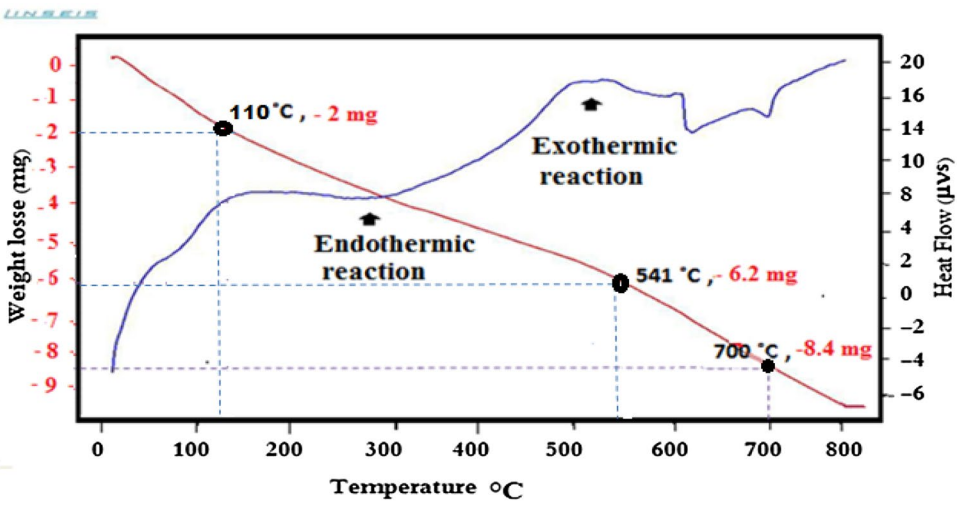

Fig. 4 Results of the TG measurements

Table 1 Indicating the value of the each mass, molar masses and mass loss as obtained at different sections of the TGA curve regions

	T (°C)	Mass (mg)	Molar mass (g\mol)	Mass loss (mg)
m_1	110	14.6136	158.05	2
m_2	541	8.4136	115.738	6.2
m_3	700	0.0136	113.541	8.4

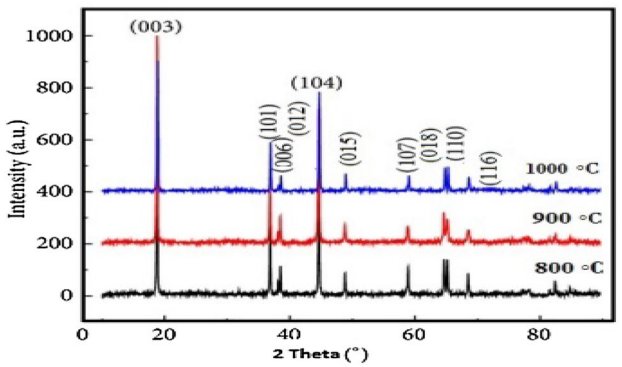

Fig. 5 XRD patterns of LCNAO nanoparticles with various annealing temperatures: 800, 900 and 1000 °C

Show these results in the calculations that the combustion powder was consist of 96.05% LCNAO 3.4% hydrocarbons, and 0.55% residual water vapor, These results agree in general with previous work on similar materials [16, 20, 21].

Based on TG analysis, it was decided to treat these powders at three different temperatures, i.e. 800, 900 and 1000 °C. Accordingly, powders were labeled P800, P900 and P1000.

Figure 5, the XRD pattern for the P800, P900 and P1000. All patterns showed high intensity peaks that indicate a good crystallinity in the annealed simples. Additionally, all samples exhibited similar peaks with slight change in positions; this will be discussed further below. All peaks can be indexed to a single phase of hexagonal lattice of space group R-3m. This emphasizes that annealing temperatures of 800 °C and above are adequate to get pure phases with insignificant impurity phases. The integrated intensity ratios of the (003)/(104) for the P800, P900 and P1000, ware 1.33, 1.335, and 1.24 respectively [15, 19]. It was not clear at this point why there was a reduction in this ratio. However, having these values of integrated intensity ratios above 1.2 generally indicates that cationic mixing between different ionic positions was small [5, 18]. The splitting of the 110 and 018 intensity lines was observed in all three patterns which Indicates the formation of the layered structure and the hexagonal lattice.

LCNAO powders grown by these wet-chemistry method displays the hexagonal oublets (006)/(102) and (018)/(110) with a clear splitting, which indicates that samples have a high degree of crystallinity, good hexagonal ordering, and greater layered characteristics. XRD results confirm the formation of pure phase [22, 23]. Characteristics of the crystalline structure emphasize that the material synthesized in the present work could be used as a cathode active compound with electrochemical properties competent to other counterparts [15].

The crystal structure of nanomaterial can greatly influence the electrochemical properties of the materials synthesized.

Elemental composition of the material was detected by X-ray energy dispersive spectroscopy (EDS), as shown in Fig. 6. The EDS results show that the weight percentages of Co, Ni and Ag were 36.52, 32.14 and 3.09 respectively. These percentages correspond to molar values of 0.5, 0.44 and 0.042 for Co, Ni and Ag respectively. Such values are in agreement with the compositional structure of the targeted material as obtained from the XRD results [16, 24–26].

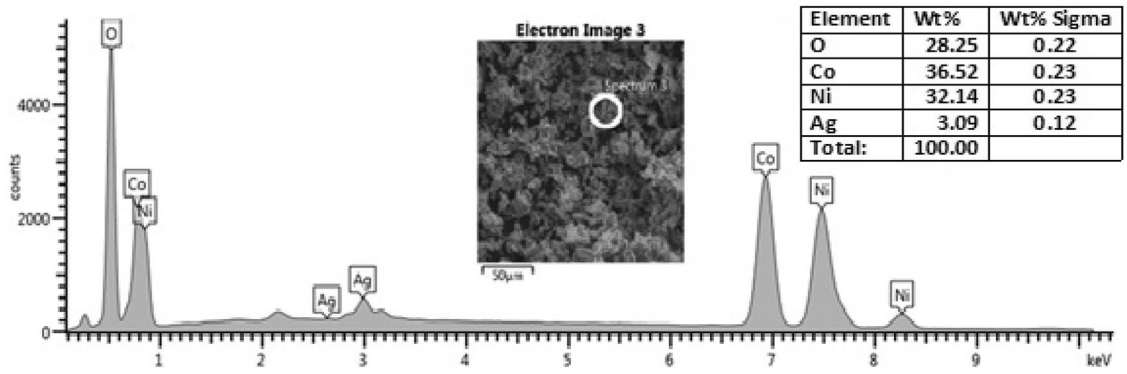

Element	Wt%	Wt% Sigma
O	28.25	0.22
Co	36.52	0.23
Ni	32.14	0.23
Ag	3.09	0.12
Total:	100.00	

Fig. 6 Energy dispersive spectrum of $LiCO_{0.5}Ni_{0.45}Ag_{0.05}O_2$ cathode active material

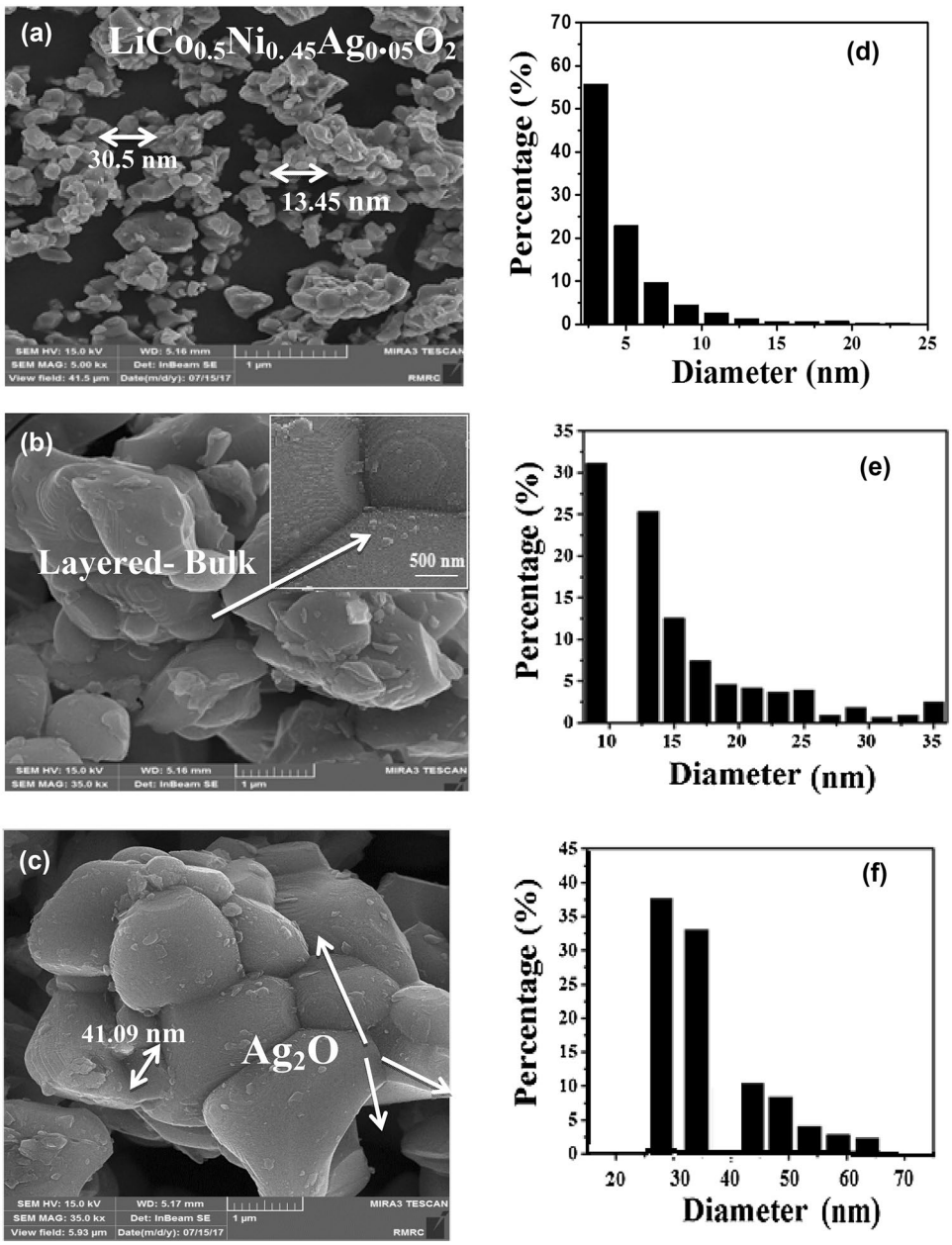

Fig. 7 FE-SEM images of the layered lithium-rich materials **a** before annealing, and after annealing (**b, c**) 800, 1000 °C. Figures **d–f** show the particle size distribution of the powders determined from the SEM micrographs

Topographic features and particle distribution in LCNAO were described by SEM images as shown in Fig. 7a–f. From these images, we observe that the particles sizes of the crystalline material formed are between 5 and 70 nm or less. These particles show a higher degree of aggregation as their sizes increase by increasing annealing temperatures of films. As shown in Fig. 7a, d, the average particle size is in the range (5–15) nm with spaces between nanoparticles

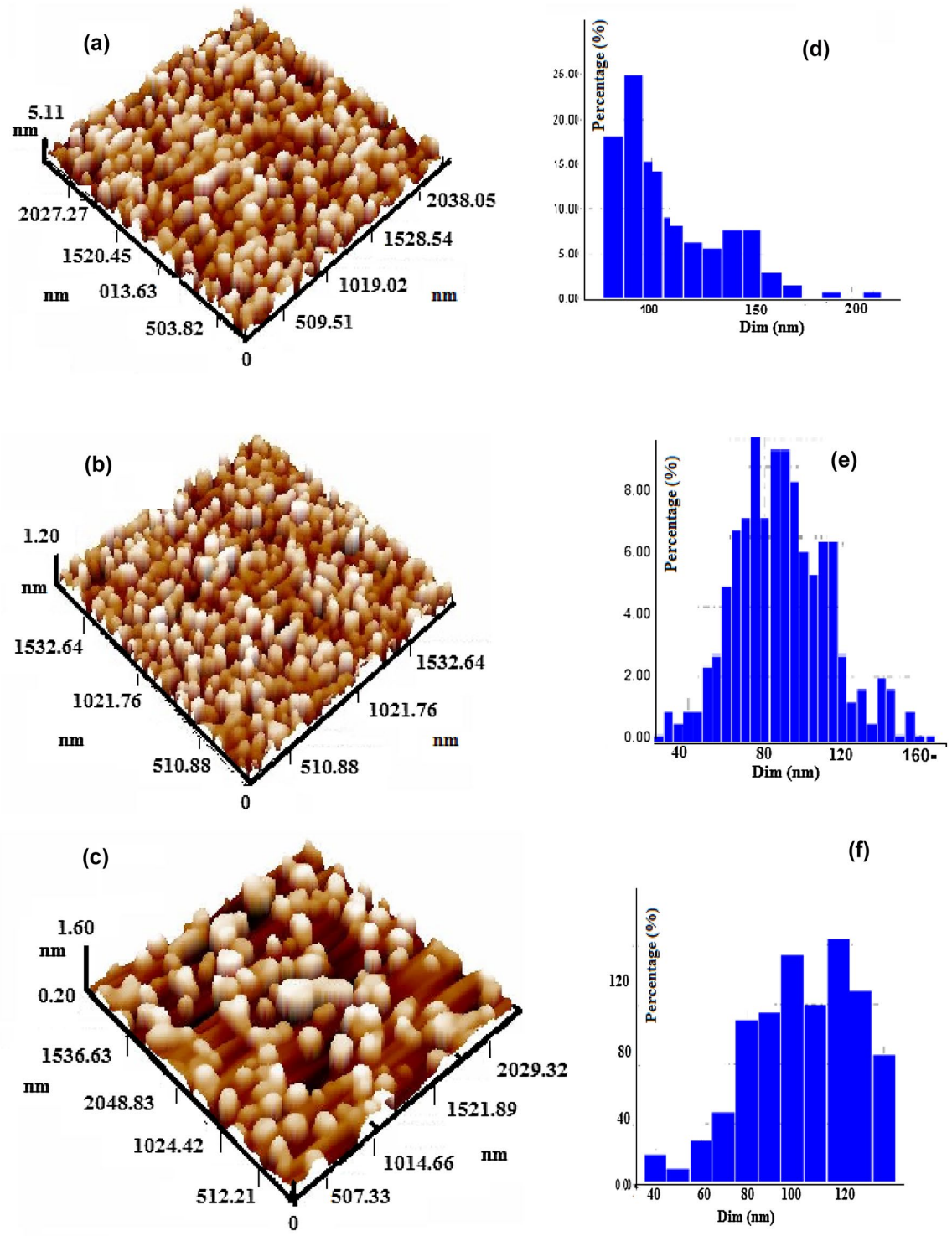

Fig. 8 3D reconstructed images of AFM micrographs and corresponding sizes distributions of $LiCo_{0.5}Ni_{0.45}Ag_{0.05}O_2$ at different annealing temperature. **a–c** 3D images of **a** 800 °C, **b** 900 °C and **c** 1000 °C. **d–f** histogram of particles size

that were irregularly spherical. When the temperature of the annealing is increased to 900 and 1000 °C, the particle size increases and the distances or spaces between the particles were decrease or finished and produce more regular and average particle size (10–30 nm) and (20–70) nm respectively as shown in Fig. 7 (b and e) and (c and f), these results were coincident with reference [26].

These images and particles histograms indicate that the material may demonstrate promising electrochemical features as intercalation and de-intercalation of Li ions is believed to improve with the decrease of diffusion distances within the material. As for our material, the condition of the crystalline structure along with the particle size and agglomeration condition present positive features to good electrochemical properties for energy storage applications test by Adawiya et al. [27].

Figure 8 shows the three dimensional constructions of the topographical structure of the active material as obtained by atomic force microscopy for the P800, P900 and P1000 powders. The area scanned in this measurement was about 2 μm × 2 μm. The topographical details, namely, the root mean square (RMS) of the surface roughness, indicate that larger particles were formed due to the increase of the annealing temperature. Surface roughness was found to increase from 0.31 nm for P800 to 0.41 nm for P1000 as shown of 3D images in Fig. 8a–c. The corresponding average particle size determined from these measurements was found to be equal to 99.1, 86 and 103.8 nm for the P800, P900 and P1000 respectively as shown in Fig. 8d–f. This increase of roughness and average particle size might be attributed to the direct effect of annealing temperature on the structure of the powders. As the temperature increases, higher energy is provided to the material and there is a higher probability to form large particles due to the increase of ion diffusion and grain formation and agglomeration [28, 29]. Table 2 summarizes the topographical features of the investigated powder in the present work.

Figure 9 shows the hysteresis Loops of LCNAO powders at different annealing temperature 800, 900, 1000 °C. The Hysteresis loops are labeled 1, 2 and 3 for the powders annealed at 800, 900 and 1000 °C respectively. As demonstrated by the VSM hysteresis loops the LCNAO prepared by combustion reaction shows good soft-magnetic properties. LCNAO nanoparticles were measured through VSM at a maximum applied field of ± 15,000 Oe (1 Oe equals about 80 A/m) at Room temperature The s Magnetic Saturation (M_s) of the samples 1, 2 and 3 are [0.70, 0.156, 0.309] emu/g respectively. The coercive force (H_c) are (41.3, 0.03, 0) Oe, the variation of Ms and H_c with the annealing temperature. The H_c increases with the annealing temperature and then decreases when the annealing temperature is higher than 900 °C. The changes in the magnetic properties of LCNAO can be attributed to the modification of the particle sizes and depends on the annealing temperature. It can be observed that all sample 1, 2 and 3 formulation reveal typical ferromagnetic behavior, close to a typical super-paramagnetic material, because M_s is at the maximum induced magnetic moment that can be obtained in a magnetic field, Hc show zero and due to changed Co^{3+}, Ni^{2+}, ion redistribution in tetrahedral and octahedral sites on heating (the decrease in the H_c with increasing $T_{annealing}$ is attributed to the grain growth) [25]. The reduced of Coercive force can be understood by the transformation from ferromagnetic to super paramagnetic state. The super-paramagnetic behavior can be attributed to the extremely fine crystalline size and regular shape of the material [28, 30, 31].

From the results, it can observed that the LCNAO powders are paramagnetic and magnetization factor gained at 0.8 emu/g in ± 15 kOe external field.

Ms, and Mr decreases with the increase in the particle size, while the Hc decreases with the increase in the annealing and heating temperature [28, 30], that is showed in Table 3.

Table 2 The topographical features of the cathode materials as obtained by AFM

Parameters LCNAO at different annealing temperature			
Parameters	800 °C	900 °C	1000 °C
Average grain diameter (nm)	99.10	86	103.82
Average Roughness (nm)	1.12	0.266	0.361
RMS (nm)	1.31	0.314	0.411
Surface (nm)	0.19	0.266	0.124

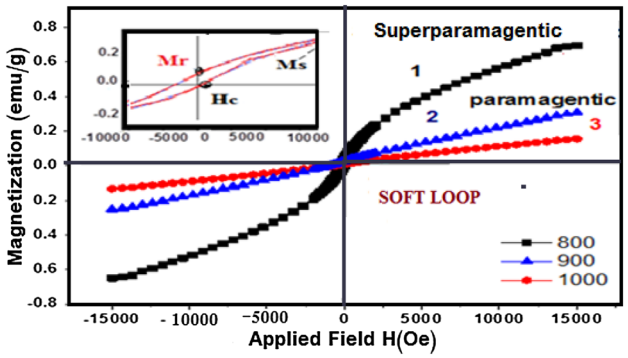

Fig. 9 Hysteresis loops of LCNAO powder annealing at 800, 900, and 1000 °C

Table 3 Ms, Mr, magnetic susceptibility (X_m) and Hc of LCNAO powder at different annealing temperature

Temperature (°C)	Average particle size (nm)	Ms (emu/g)	Mr (emu/g)	$X_m = Mr - 1$ (emu/g)	Hc (kOe)
800	99.10	0.70	0.052	−0.948	41.3
900	86	0.156	0.0119	−0.9881	0.034
1000	103.82	0.309	0.027	−0.973	0

4 Conclusion

Silver doped and lithiated transition metal oxide of the form of $LiCo_{0.5}Ni_{0.45}Ag_{0.05}O_2$ was successfully synthesized by combustion reaction for cathodes of lithium–ion batteries. The structural and compositional investigations have confirmed the possibility to synthesize these materials in layered structure of high crystallinity and well-defined compositions. The post synthesis processing was established through the investigation of the annealing temperature on the Topographical, structural and compositional characteristics of the material. The synthesized material is believed to be a potential candidate and competing material for energy storage application in lithium–ion batteries. The prepared samples exhibit ferromagnetism nature of all samples at room temperature with clear hysteresis loops. The coercive force is strongly dependent not only on annealing temperature but also surface roughness.

Acknowledgements The authors gratefully acknowledge the technical support provided by the Applied Science Department, Laser and Chemical Branch, University of Technology, and Baghdad, Iraq.

References

1. J. Christian, M. Alain, V. Ashok, Z. Karim, *Lithium Batteries Science and Technology* (Springer, New York, 2016). ISBN 978-3-319-19108-9
2. J.M. Tarascon, Key challenges in future Li-battery research. Philos. Trans. R. Soc. Lond. A, **368**(1923), 3227–3241 (2010)
3. V.P. Patil, S. Pawar, M. Chougule, P. Godse, R. Sakhare, S. Sen, P. Joshi, Effect of annealing on structural, morphological, electrical and optical studies of nickel oxide thin films. J. Surf. Eng. Mater. Adv. Technol. **1**(02), 35 (2011)
4. J.M. Zheng, X.B. Wu, Y. Yang, A comparison of preparation method on the electrochemical performance of cathode material $Li[Li_{0.2}Mn_{0.54}Ni_{0.13}Co_{0.13}]O_2$ for lithium ion battery. Electrochim. Acta **56**(8), 3071–3078 (2011)
5. A.A.A. Al-Tabbakh, N. Kamarulzaman, A.S. AL-Zubaidi, Synthesis and properties of a spinel cathode material for lithium ion battery with flat potential plateau. Turk. J. Phys. **39**(2), 187 (2015)
6. B. Zhang, Z. Wang, H. Guo, Effect of annealing treatment on electrochemical property of $LiNi_{0.5}Mn_{1.5}O_4$ spinel. Trans. Nonferrous Met. Soc. China **17**(2), 287–290 (2007)
7. N.W.B. Balasooriya, P.W.S.K. Bandaranayake, Electrochemical properties of $LiCo_{0.4}Ni_{0.6}O_2$ and its performances in rechargeable lithium batteries. Sri Lankan J. Phys. **8**, 47–58 (2007)
8. Q. Liug, Y. Wang, H. Chen, Synthesis and electrochemical performance of $LiNi_{0.5}Mn_{1.5}O_4$ spinel compound. Electrochim. Acta **50**, 1965–1968 (2005)
9. J. Kim, S.T. Myung, Y.K. Sun, Molten salt synthesis of $LiNi_{0.5}Mn_{1.5}O_4$ spinel for 5V class cathode material of Li-ion secondary battery. Electrochim. Acta **49**, 219–227 (2004)
10. S.T. Myung, S. Komaba, I.N. Kumaga, O.H. Yashir, H.T. Chung, T.H. Cho, Nano-crystalline $LiNi_{0.5}Mn_{1.5}O_4$ synthesized by emulsion drying method. Electrochim. Acta **47**, 2543–2549 (2002)
11. Q. Sun, X. Li, Z. Wang, Y. Ji, Synthesis and electrochemical properties of 5V spinel $LiNi_{0.5}Mn_{1.5}O_4$ cathode materials prepared by ultrasonic spray pyrolysis method. Nonferrous Met. Soc. China **19**, 176–181 (2009)
12. J.C. Arrebola, A. Caballero, Crystallinity control of a nanostructured $LiNi_{0.5}Mn_{1.5}O_4$ spinel via polymer-assisted synthesis: a method for improving its rate capability and performance in 5V lithium batteries. Adv. Funct. Mater. **16**, 1904–1912 (2006)
13. H. Xia, S.Y. Meng, L. Lu, G. Ceder, Electrochemical behavior and Li diffusion study of $LiCoO_2$ thin film electrodes prepared by PLD. J. Power Sources **159**, 1422–1427 (2006)
14. Y. Ding, P. Zhang, Y. Jiang, D. Gao, Effect of rare earth elements doping on structure and electrochemical properties of $LiNi_{1/3}Co_{1/3}Mn_{1/3}O_2$ for lithium-ion battery. Solid State Ion. **178**(13), 967–971 (2007)
15. J. Zhu, *Synthesis, Characterization and Performance of Cathodes for Lithium Ion Batteries* (Ph.D. University of California, 2014), pp. 31–45
16. J.H. Adawiya, A.R. Rusul, J.H. Mohammad, Morphological and structural properties of cathode compound material for lithium-ion battery. Plasmonics **8**(3), 1–9 (2018)
17. J. Adawiya, A. Rusul, A. Ahmed, M. Nasser, in *Structural, Morphological and Optical Properties of* $LiCo_{0.5}Ni_{0.45}Ag_{0.05}O_2$ *Thin films*, International Conference of TMREES18- Beirut, Lebanon, Journal of AIP Conference Proceedings, 1968, 020001 (2018)
18. H.J. Bergveld, V. Pop, P.P.L. Regtien, J.H.G. Op het Veld, D. Danilov, P.H.L. Notten, Battery aging and its influence on the electromotive force. J. Electrochem. Soc. **154**(8), A744–A750 (2007)
19. J.L. Shi et al., High-capacity cathode material with high voltage for Li-Ion batteries. Adv. Mat. (2018). https://doi.org/10.1002/adma.201705575
20. C. Julien, A. Mauger, A. Vijh, K. Zaghib, *Lithium Batteries* (Springer, New York, 2016), pp. 29–68
21. Y. Aykut, B. Pourdeyhimi, S.A. Khan, Synthesis and characterization of silver/lithium cobalt oxide ($Ag/LiCoO_2$) nanofibers via sol–gel electrospinning. J. Phys. Chem. Solids **74**(11), 1538–1545 (2013)
22. Z.M. Gao, Y.Y. Liu, F. Lin, L.H. Dang, L.J. Wen, EIS characteristic under cathodic protection and effect of applied cathodic

potential on surface microhardness of Q235 steel. Int. J. Electrochem. Sci. **8**(8), 10446–10453 (2013)
23. G. Xu et al., Prescribing functional additives for treating the poor performances of high-voltage (5 V-class) $LiNi_{0.5}Mn_{1.5}O_4$/MCMB Li-ion batteries. Adv. Energy Mater. **8**(9), 1701398 (2018)
24. A.L.B. Daniel, H. Wulfmeier, F. Holger, Preparation and characterization of c-$LiMn_2O_4$ thin films prepared by PLD for lithium-ion batteries. Eng. Technol. **4**, 1558–1564 (2016)
25. M. Park, X. Zhang, M. Chunga, G.B. Less, A. Marie Sastry, A review of conduction phenomena in Li-ion batteries. J. Power Sources 195(24):7904–7929 (2010)
26. B. Philippe, A. Mahmoud, J.B. Ledeuil, M.T. Sougrati, K. Edström, R. Dedryvère, P.E. Lippens, $MnSn_2$ electrodes for Li-ion batteries: mechanisms at the nano scale and electrode/electrolyte interface. Electrochim. Acta **123**, 72–83 (2014)
27. J.H. Adawiya, A.R. Rusul, Q.A. Ahmed Electrical properties and electrochemical impedance spectroscopy for $LiCo_{0.5}Ni_{0.45}Ag_{0.05}O_2$ powder, (ICASE) International Conference on Advances in Sustainable Engineering and Applications, March (2018)
28. X. Hui, L. Li, Growth of layered $LiNi_{0.5}Mn_{0.5}O_2$ thin films by pulsed laser depositio for application in microbatteries. Appl. Phys. Lett. **92**, 011912 (2008)
29. P. Balakrishnan, P. Veluchamy, Synthesis and characterization of $CoFe_2O_4$ magnetic nanoparticles using sol-gel method. Int. J. ChemTech Res. **8**(1), 271–276 (2015)
30. C. Juliena, C. Letranchanta, S. Rangana, M. Lemala, Layered $LiNi_{0.5}Co_{0.5}O_2$ cathode materials grown by soft-chemistry via various solution methods. Mater. Sci. Eng. B **76**(2), 145–155 (2000)
31. C. Julien, A. Mauger, K. Zaghib, H. Groult, Optimization of layered cathode materials for lithium-ion batteries. Materials **9**(7), 595 (2016)